Strong geomagnetic activity forecast by neural networks under dominant southern orientation of the interplanetary magnetic field

Fridrich Valach

Geomagnetic Observatory, Geophysical Institute, Slovak Academy of Sciences, Komárňanská 108, 947 01 Hurbanovo, Slovakia

Josef Bochníček and Pavel Hejda

Institute of Geophysics, Academy of Sciences of the Czech Republic, Boční II/1401, 14131 Prague, Czech Republic

Miloš Revallo

Geophysical Institute, Slovak Academy of Sciences, Dúbravská cesta 9, 845 28 Bratislava, Slovakia

Abstract

The paper deals with the relation of the southern orientation of the north-south component B_z of the interplanetary magnetic field to geomagnetic activity (GA) and subsequently a method is suggested of using the found facts to forecast potentially dangerous high GA. We have found that on a day with very high GA hourly averages of B_z with a negative sign occur at least 16 times in typical cases. Since it is very difficult to estimate the orientation of B_z in the immediate vicinity of the Earth one day or even a few days in advance, we have suggested using a neural-network model, which assumes the worse of the possibilities to forecast the danger of high GA - the dominant southern orientation of the interplanetary magnetic field. The input quantities of the proposed model were information about X-ray flares, type II and IV radio bursts as well as information about coronal mass ejections (CME). In comparing the GA forecasts with observations, we obtain

Email addresses: `fridrich@geomag.sk` (Fridrich Valach), `jboch@ig.cas.cz and ph@ig.cas.cz` (Josef Bochníček and Pavel Hejda), `geofmire@savba.sk` (Miloš Revallo)

Preprint submitted to Advances in Space Research *December 2, 2013*

values of the Hanssen-Kuiper skill score ranging from 0.463 to 0.727, which are usual values for similar forecasts of space weather. The proposed model provides forecasts of potentially dangerous high geomagnetic activity should the interplanetary CME (ICME), the originator of geomagnetic storms, hit the Earth under the most unfavorable configuration of cosmic magnetic fields. We cannot know in advance whether the unfavorable configuration is going to occur or not; we just know that it will occur with the probability of 31%.

Keywords: geomagnetic activity; interplanetary magnetic field; artificial neural network; ejection of coronal mass; X-ray flares

---

1. Introduction

It is generally accepted that the southern orientation of the north-south component B_z of the interplanetary magnetic field (IMF) enables strong geomagnetic storms to develop. This is so because such configuration of magnetic fields enables the IMF lines of force to connect up with the lines of force of the geomagnetic field. This enables magnetic sub-storms to develop and, under strongly disturbed solar wind conditions, e.g., CME or ICME, the development of geomagnetic storms. Many authors have studied the association of the occurrence of a southerly oriented IMF and geomagnetic disturbances. It was found that, for the generation of strong geomagnetic storms, it is important that the southern B_z be sufficiently large and simultaneously of sufficient duration. Tsurutani (2001), e.g., arrived at the conclusion that B_z should drop below -10 nT for at least three hours.

Although we know that the orientation of B_z is very important for GA, GA forecasters face the problem in connection with B_z that, for the purpose of mid-tem forecasts, they are unable to estimate the orientation of the IMF with sufficient accuracy for one or a few days in advance. The information required about the IMF would be that in sheet plasma behind shocks, as well as in ejection clouds. However, in the former case the orientation of B_z appears to be random, since during some events the southern component does not occur at all, whereas in other events the southern B_z last for several hours (Schwenn, 2006). So far we do not have sufficient information about the topology of ejecta clouds (Schwenn, 2006) although it has already been established that the orientation and helicity of filaments before the eruption is often reflected in the topology of the resulting magnetic clouds (Bothmer & Schwenn, 1998; Yurchyshyn et al., 2001). They suggested that these facts be used in optimizing the forecasts of geomagnetic effects, e.g., McAllister et al. (2001) and Zhao et al. (2001). On the other hand, Chen et al. (1996, 2012) used Bayesian approach and developed the algorithm which uses real-time solar wind magnetic data obtained at the L1 Lagrange point to predict the magnetic field structure of the upstream solar wind that has yet to arrive, and its geoeffectiveness. Their tests show that the average warning time for the magnetic storm ranges from a few hours to a maximum of 10-15 hours.

In near-real time forecasts, the information about B_z is usually one of the input data, e.g., (Boberg et al., 2000; Lundstedt et al., 2002; Jankovičová et al., 2002). A certain disadvantage of these forecasts is usually the short lead time, which usually amounts to one or a few hours. This is roughly the time which the plasma of the disturbed solar wind requires for traveling from the libration point, where B_z is measured by satellites, to the Earth plus the time required for the geomagnetic disturbance to develop. That is why we speak of near-real time forecasts.

Long-term forecasts, in which the time scale is months or years, involve rather space climatology which, among others, makes use of cyclic manifestations of solar and geomagnetic activity. The orientation of B_z during the individual geomagnetic storms plays no significant part in such forecasts.

As regards practical purposes, e.g., the safety of space travel, intercontinental air travel or operation of electricity distribution networks, most suitable are GA forecasts, in which the leading time is days, i.e. mid-term forecasts. From a practical point of view, it is necessary to concentrate on very strong geomagnetic storms. That is the reason why it is necessary to study the relations between the orientation of B_z and the high level of geomagnetic activity. The findings then have to be utilized for practical purposes in forecasts space weather. This paper is devoted to these two problems. In Section 2, we shall study the geomagnetic activity expressed in terms of geomagnetic index C9 in relation to the orientation of B_z, and in Section 3 we shall out line one of the possibilities of making use of the facts obtained about B_z in mid-term forecasting with the aid of artificial neural networks.

It is important to emphasize that in this paper we are dealing with a model, the time scale of which is days. That is why we have used the daily index C9 as the measure of geomagnetic activity. This index provides a qualitative estimate of overall level of magnetic activity for the day determined from the sum of the eight Ap amplitudes, which are directly related to the well-known Kp index. It is given by one digit between 0 (quiet) and 9 (highly disturbed).

The use of the time scale of days has its justification. We consider CME's to be the main cause of enhanced geomagnetic activity. The CME observed close to the Sun will last one to four days, while the appropriate ICME (i.e. the interplanetary "continuation" of the CME) travels the distance of one Astronomical Unit (Schwenn, 2006).

It might seem that only the fastest propagating CME/ICME's are most important for enhanced geomagnetic activity. For example, only 17 hours and 40 minutes elapsed between the time the famous and extremely strong Carrington solar flare was observed and the commencement of the subsequent strong geomagnetic storm. This was the first solar flare observed. It was discovered also due to its exceptional intensity by R.C. Carrington, and it was also independently observed by R. Hogson on Sept. 1, 1859 (Schwenn, 2006). In the above case, we assume that a rapidly propagating CME, which caused the geomagnetic storm, was associated with this solar flare.

However, Tsurutani et al. (2004) analyzed slow magnetic clouds which were also surprisingly geo-effective. For example, the well-known event of Jan. 6, 1997, when a slow partial halo CME caused a very strong storm with widespread effects on Earth only after 85 hours (Tsurutani et al., 2004). That is why Schwenn (2006) says that space weather forecasters have to come to terms with the 24-hour uncertainty of the arrival of the CME.

The forecast of the orientation of the IMF in the vicinity of the Earth is problematic and, from a practical point of view, it appears more convenient to accept that it is unpredictable and to adjust our approach to forecasting GA accordingly. Nevertheless, it is necessary to continue the studies which will enable us to forecast B_z in the future. The purpose of this paper is to suggest one possible approach to forecasting strong GA under the simplified assumption that the orientation of the IMF is unpredictable.

2. Vertical component of the IMF and geomagnetic activity

The purpose of this section of the paper is to determine the statistical relationship between the southern orientation of the IMF and the occurrence of days with high GA. Data sources are briefly described and followed by statistical analysis based on quantile characteristics.

2.1. Data used

In this study, the IMF is expressed in terms of hourly averages of the vertical component, B_z, measured by the ACE satellite at libration point L1. The data were adopted from the web site of the ACE Science Center

Fridrich Valach, Josef Bochníček, Pavel Hejda and Miloš Revallo: Strong geomagnetic activity forecast by neural networks under dominant southern orientation of the interplanetary magnetic field.
Advances in Space Research, VOL 53, ISSUE 4, PAGES 589-598, 2014. DOI: 10.1016/j.asr.2013.12.005

(ACE, 2012). For our purposes we have used the data available as of Sept. 2, 1997 to the end of 2007, which cover nearly the whole of the 23rd solar activity cycle. Some data gaps occurred in the records of the IMF; therefore, we excluded all the days with incomplete data from our analysis.

The geomagnetic activity was characterized by the C9 index. We have explained the choice of this index in Section 1. The source of the geomagnetic data was the National Geophysical Data Center (NGDC, 2012) and the data were adopted from the same time period as for the B_z data, i.e. from Sept. 2, 1997 to Dec. 31, 2007.

2.2. Occurrence of GA levels for various durations of negative B_z

We have used quantile characteristics to describe the occurrence of GA levels for various durations of negative B_z, because this description is the more natural than moment characteristics for discrete values of the number of hours and the C9 index.

The key result of this relatively simple survey analysis of data is the number of hours in a given day, when B_z was negative. The statistics was made separately for the individual GA levels on the given day, i.e. separately for C9 = 0, 1, 2, ..., 9. It was found (Fig. 1) that for the majority of days with very high GA (C9 = 8 or 9) B_z was negative for at least sixteen hours. For days on which the activity C9 = 7, this 16-hour threshold value of the occurrence of negative B_z is just the median. This means that a typical day with activity C9 = 7 has 16 hours in which $B_z < 0$.

The next analysis (Fig. 2) shows that, on days on which the hourly average of B_z was negative at least 16 times, the GA was higher (the median of index C9 is 3) than in the other cases (median of C9 is 2). In view of the assumed role of the negative value of the north-south component of the IMF, this result was only to be expected.

The significance of the above conclusions is in that there is at least the possibility of restricting ourselves in forecasting GA to the more dangerous case when B_z is at least negative for 16 hours, if we assume that we are unable to sufficiently forecast the orientation of B_z at libration point L1. This forecast will then represent the more dangerous of the possible evolutions. We have analyzed 2882 days, of which 891 days (i.e. 31 per cent) were "dangerous" days, on which such scenario can materialize.

Practically, the warning published against the danger of very high GA could, e.g., read as follows: "A pronounced CME has been emitted from the Sun towards the Earth. Should southern orientation of the IMF be maintained for a longer period after the arrival of the ICME at the Earth, a strong geomagnetic storm with index C9 equal to 8 or 9 could occur within the next few days. The probability of occurrence of the southern orientation of the IMF is 31 per cent".

One of the possibilities of realizing such forecast is described in the following section (Section 3).

3. The neural-network model of forecasting the danger of strong GA

The existing models, which have based forecasting of GA on CME data or solar-flare data, have either not considered the problem of poor predictability, or unpredictability of the sign of the north-south component of the IMF, or have included the B_z-values among the input parameters. In the former case, this resulted in the lesser agreement of the forecast with observations, in the latter case the forecast became short-term or near-real time forecasts.

The process we have proposed, in which we forecast the danger of strong GA should conditions favorable for its development with regard to the orientation of the IMF exist, is a mid-term forecast. It is based on the application of neural networks (NNs). To be able to repeat our process, or for other authors to be able to improve it, it is necessary to describe the form of the input parameters we used, and also to specify the architecture of the NNs used. The next three sub-sections (Sub-sections 3.1, 3.2 and 3.3) are devoted to these problems. The result of the modeling of NNs and their comparison with the NN models of other authors will be the subject of Section 4.

3.1. Input data for the NN model

In deciding on which input parameters we shall use in our model, we drew on the models hitherto published on forecasting space weather. Valach et al. (2007) used information on the classes of X-ray flares (classes B, C, M and X), on heliographic position of the sources of these flares to predict GA, as well as information on whether the X-ray flare was accompanied by type II or IV radio bursts. Other authors used CME data. For example, Gleisner & Watermann (2006a,b) used CME data together with information on high-energy proton fluxes (HEPF > 10 MeV). Such input parameters improve the reliability of the GA forecast, however, the necessity of information on the HEPF slight shortens the lead time as solar energetic particles (SEPs) are observed with a certain time delay after the CME onset. Srivastava (2005) considered the latitude of the origin of the CME, as well as the longitude, which she combined into a simple binary variable, which she called the source location. A CME, which occurred inside the region ±40° latitude and ±40° longitude, is considered more geo-effective in her model than a CME, which occurred outside this region. This agrees with the results of Bochníček et al. (2007) and Valach et al. (2007) who came to the conclusion that more geo-effective are more probably the solar energetic events which originated close to the center of the solar disc.

As regards our model of forecasting the danger of strong GA, we chose the following input quantities which we used to characterize the individual days:

1. The position angle[1] of the most significant CME, which occurred on the given day. In this study we restricted ourselves to full and partial halo CMEs, a CME whose width exceeded 140° being considered a partial halo CME. We considered more significant CMEs whose widths were larger. The position angle is not determined for full halo CMEs. That is why, in our database, we assigned it a special value (-360°).
2. The largest CME width observed on the given day.
3. The linear velocity of the most significant CME.
4. The total number of CMEs observed on the given day, which were either partial or full halo.
5. The class of the most significant X-ray flare (XRA class) which was observed close to the solar disc center (±40°) on the given day. The most significant X-ray flare was determine in accord with the results of Bochníček et al. (2007) and Valach et al. (2007). The first and most important feature of the most significant flare is that it was accompanied by a type IV radio burst. The second, less important criterion is that the more significant flare was classified as a flare of higher class. In our study we only consider class B and higher classes. The third, least important criterion was that the flare was accompanied by a type II radio burst.
6. Information on whether a type IV radio burst was observed in connection with the most significant X-ray flare on the given day.

[1] The angle projected into the sky plane, which is measured from the northward vector in a solar or heliospheric image. It begins at zero degrees (north) and moves counterclockwise toward the east (Howard, 2011).

7. Information on whether a type II radio burst was observed in connection with the most significant X-ray flare on the given day.
8. Number of X-ray flares observed close to the solar disc center ($\pm 40^{\circ}$) on the given day.

If no partial or full halo CME was observed on any day, the first four quantities in the above list of inputs were put equal to zero. If no X-ray flare of at least class B was observed on any day, the last four quantities in the above list were put equal to zero on the given day.

The CME data were adopted from the SOHO/LASCO Catalogue (Gopalswamy et al., 2009; Gopalswamy & Yashiro, 2012). The Catalogue is generated and maintained at the CDAW Data Center by NASA and The Catholic University of America in cooperation with the Naval Research Laboratory. SOHO is a project of international cooperation between ESA and NASA. The source of information on X-ray flares were the daily bulletins issued by the NOAA Space Environment Center, Boulder, Colorado, USA (SWCP, 2012).

In this way we employed some pieces of information about CMEs, which are the recognized causes of the strong magnetic storms (Howard, 2011), together with the data about the data on the X-ray flares accompanied by solar radio bursts (RSP) of Type II, interpreted as the signature of shock wave initiation in the solar corona, and Type IV, representing upward-moving material in corona (Kosugi & Shibata, 1997). This procedure is justified by the fact that the growing observations support the point that flares and CME are two phenomena in one process just as suggested by Harrison (1996), Dryer (1996), Kosugi & Shibata (1997), Cliver & Hudson (2002), and Howard (2011).

The eight defined input quantities proved their worth in a similar manner also in modeling SEP events, which was published in (Valach et al., 2011).

The forecast quantities, i.e. output quantities provided by our model, were the value of the C9 index. In this part of our study, we considered 468 days, for which all the necessary data from CME observations and also X-ray flares were available. These data were all from the period 1998 to 2005, years of the solar maximum with frequent CME occurrences. During this period, full or partial halo CMEs appeared approximately once every 36 hours (Valach et al., 2011).

The input and output data described above served to feed the artificial neural network, which is the tool described in the next sub-section.

3.2. The artificial neural-network method

One of the widely used tools in forecasting is the artificial neural network (NN). One of the general definitions of the NN, given by Gurney (1997), is: "A Neural Network is an interconnected assembly of single processing elements, units or nodes, whose functionality is loosely based on the animal neuron. The processing ability of the network is stored in the interunit connection strengths, or weights, obtain by a process of adaptation to, or learning from, a set of training patterns". The NNs have been used by a number of authors also in forecasting GA, e.g., (Andrejkova et al., 1998; Boberg et al., 2000; Chen et al., 1996, 2012; Jankovičová et al., 2002; Kugblenu et al., 1999; Lundstedt & Wintoft, 1994; Lundstedt et al., 2002; Stepanova et al., 2008; Tian et al., 2005; Valach et al., 2007, 2009; Wu, 1997). The theory of neural network is described in detail in many textbooks, e.g., (Gurney, 1997; Hertz et al., 1991). In this paper, we have used a three-layer neural network with forward propagation, which had the following architecture:

The 1st layer of neurons, the input layer, consisted of 32 input neurons. They were connected to eight input quantities according to the list in Sub-section 3.1, in each case for four consecutive days. We chose the four-day span for input sequence because the geoeffective CMEs typically need from one to four days to reach the Earth after their onsets. Thus, in order to forecast the GA, we require information about the course of events occured in space during four days before the day in question. Hence the above mentioned pattern is a sequence of data from five days: four consecutive days of the input data and the fifth day, for which the GA is forecast. The patterns which follow one after the other are overlapping – the next pattern is constructed from the days which are shifted by one day.

The 2nd layer was the so-called hidden layer. It consisted of hidden neurons, the number H of which had to be determined by the validation test. This test will be described later (Sub-section 3.3).

The 3rd layer, the output layer, was represented by a single output neuron. The output of this neuron is the forecast value of the C9 index for the day immediately following the four days, the values of which (i.e. both CME and X-ray flare data described in Sub-section 3.1) were put into the input layer (Fig. 3). If the input quantities are marked as vector $\vec{x} = [x_1, x_2, ..., x_{32}]$ the output of our neural network should read:

$$y = f\Big(\sum_{j=1}^{H} W_j \cdot f\Big(\sum_{l=1}^{32} w_{j,l} \cdot x_l - w_{j,0}\Big)\Big), \qquad (1)$$

where W_j, $w_{j,l}$ and $w_{j,0}$ are the interunit connection strengths, or weights, in which the processing ability of the network is stored, as already mentioned above. The letter f stands for the activation function, which in this study is $f(z) = 1/(1 + exp(-z))$.

Let us assume that there are M input vectors. We can then define the mean square error as

$$MSE = \sum_{m=1}^{M} (y_m^{out} - y_m^{pred})^2/M, \tag{2}$$

where y_m^{out} stands for the required output of the NN and y_m^{pred} is the actually obtained output. The NN is trained to yield a minimum MSE. The next sub-section describes the process of training the neural network.

3.3. Training and validation of neural networks

To obtain the values of weights W_j, $w_{j,l}$ and $w_{j,0}$, for which the MSE is minimum, for a neural network with a given number of hidden neurons H, we had to train the network. For this purpose, it was necessary to have training data (patterns) and an algorithm for adapting the weights. Several algorithms for training neural networks have been developed, e.g., (Demuth et al., 2005-2007). In this paper we have used the backpropagation (BP) algorithm, based on the generalized delta rule and improved by an inertial term (Gurney, 1997).

However, determining just the suitable weights for the neural network with a single "guessed" number H was not enough. It was necessary to test various neural networks, which had different numbers of hidden neurons. We compared the prediction abilities of the individual neural networks after training them. This comparison of the results of the neural networks, so-called validation test, was carried out on other patterns than the patterns used to train the networks.

Besides, we reserved a certain number of data for the final test. In the independent final test, we then made a forecast (post factum) on the independent patterns, which had been used neither for training, nor for the validation test.

There is no common opinion as to the ratio in which the training, validation and independent testing patterns should be represented. Schmid (2009) recommended the ratio of 3:1:2. We divided the patterns in the recommended ratio by random selection with the aid of a random number generator. We thus obtained 234 training patterns, 78 validation patterns and 156 testing patterns for the final test.

The number of hidden neurons H in our NNs was changed in the range from 1 to 64. The BP algorithm is a numerical iteration method, the first step of which is setting the initial values of the weights to small random numbers. Some selected parameters also occur in the algorithm: rate of learning[2] (we chose the value 0.1) and the momentum constant[3] (we worked with the value 0.6). The result of the training may to some extent be affected by these initial settings. That is why we ran ten trainings for every value H. We thus compared the results of as many as 640 neural networks in the validation test.

The purpose of the validation test was to identify several networks with the best ability to forecast strong GA. We chose 36 networks, which yielded the best results with a view to the Hanssen-Kuiper skill score (KSS). The KSS is also known as the true skill statistic (TSS) and is defined by the relation

$$KSS = TSS = \frac{ad - bc}{(a + c)(b + d)} \ , \tag{3}$$

where a is the number of hits (correctly forecast strong GA which really did occur), b the number of false alarms, c the number of lacking warnings and d the number of correct non-event forecasts. KSS takes values between -1 to 1. Value 1 stands for perfect score, whereas value 0 stands for no skill level. KSS evaluates the successfulness of "yes/no"-type forecasts. In seeking the best neural networks for forecasting strong GA, we defined the meaning of strong GA in three different ways, i.e. what "yes" means in our statistics:

1. High GA occurs if C9 is at least 7.
2. GA is high if C9 is 8 or 9.
3. GA is considered high only if C9 is 9.

Besides the demand on the highest values of KSS for the selected neural networks, we sought comparable representation of networks designated

[2]A parameter which governs how big the changes to the weights during the trainig process are and, hence, how fast the learning takes place (Gurney, 1997).

[3]This constant multiplied by the previous weight change is called momentum term. The therm is added to the next weight change, which is computed according to BP algorithm, in order to speed convergence and avoiding instability of the training process (Gurney, 1997).

according to the three definitions of the strong GA. Following the first definition, 12 networks were designated. The second and the third definitions yielded 13 and 17 networks, respectively, yet 6 of them were simultaneously designated by both the definitions. Thus 36 various neural networks were selected, all told.

We considered the medians of the outputs of the selected 36 neural networks to be the resultant NN model.

It seems that the higher the GA we are trying to identify, the simpler the appropriate neural network (Fig. 4). However, we must not overvalue this conclusion, because GA with C9 equal to 9 was observed in the test models only three times.

4. Evaluation of the independent test

With the aid of the training and validation patterns, of which there were 312, we created a neural-network model consisting of 36 neural networks. We reserved 156 patterns to test it. These were randomly chosen patterns, which were not used in training or validation and which served exclusively for the independent final test of the successfulness of the forecast.

The results of the test (Table 3) showed that, in spite of the relatively large number of neurons in the hidden layer (Fig. 4) our model had a very limited ability to distinguish the degrees of GA, if medium or low GA was involved (C9 < 7). This is not surprising, because the validation test was focused only on the magnetically most disturbed days (C9 ≥ 7). This agrees with the purpose of forecasting high GA we declared. Figure 4 indicates that the forecasting of lower levels of GA would probably require neural networks with a very large number of hidden neurons H, which would also be associated with a much larger database of patterns. These are not yet available. However, we doubt that an increase in H over and above 64 would lead to improvement, since the published NN models for forecasting GA, e.g., (Boberg et al., 2000; Jankovičová et al., 2002; Lundstedt & Wintoft, 1994; Lundstedt et al., 2002; Valach et al., 2007, 2009) contain hidden layers with roughly 10 hidden neurons, or also less. For this reason, our intention to concentrate on forecasting high GA was reasonable.

The advantage of our NN model is that it is able forecast whether the GA on the given day will be high (C9 ≥ 7) or not. In assessing the successfulness of these categorical forecasts, we have become used to use, apart from the KSS or TSS (see Eq. 3) some other scores such as the probability of detection $POD = a/(a+c)$, the false alarm rate $F = b/(b+d)$, or proportion correct $PC = (a+d)/(a+b+c+d)$. What quantities a, b, c and d stand for, was explained in Sub-section 3.3. The range for the scores POD, F and PC is 0 to 1, the value 1 being the perfect score for PC and POD, and, on the contrary, 0 is the perfect score for the false alarm.

The scores for the case in which we considered C9 = 7 to 9 to be high GA, which we wish to forecast, are shown in Table 1. The same indices for high GA, defined as C9 = 8 or 9, are in Table 2. With the exception of POD and KSS for "yes", defined as C9 = 7 to 9 (Table 1) which are equal to 0.500 and 0.463, respectively, all the other scores were close to the required values. Proportion correct in both cases and also POD in the second case (Table 2) were close to unity. On the contrary, the false alarm rates (Fs) were close to zero in both cases.

As regards the comparison of KSS with the results of other studies, we mention that the usual value of KSS in predicting SEP events based on the same input quantities as used in this paper, was 0.54 [4] (Valach et al., 2011).

This indicates that our model provides forecasts with standard successfulness. The drawback of the above statistics is the small number of days with high GA, but very severe geomagnetic storms are not a frequent event. Moreover, we had to use most of the days with high GA to determine the weights and architecture (values of H) of the neural networks.

At this point we shall mention the comparison with other NN models of mid-term forecasts of GA, the input parameters of which agreed only in part with our inputs, and the output value of GA was also defined differently. Valach et al. (2007) published a NN model in which the input data were only X-ray flares accompanied be type II or IV radio bursts. In forecasting severe geomagnetic storms, these authors arrived at results for which we have calculated the following skill scores: $KSS = 0.265$, $POD = 0.578$, $F = 0.312$ and $PC = 0.634$. Once the solar energetic particle (SEP) flux was added to these input data, the skill scores improved. We calculated that their $KSS = 0.435$, $POD = 0.478$, $F = 0.043$ and $PC = 0.717$. Srivastava (2005) published a logistic regression model which was similar to NN modeling. Apart from the information on CMEs, solar flares and their positions on the solar disc,

[4] The value 0.54 is the median of the values mentioned in (Valach et al., 2011). The lower quartile for the KSS, mentioned in the paper referred to, was 0.45, the upper quartile 0.69. The authors also calculated the KSS for a similar study by Kahler et al. (2007). They also obtained KSS = 0.54.

she considered also information about the solar wind and the IMF measured at libration point L1. Her model was trained to classify geomagnetic storms into two categories: intense and super-intense storms. For her study we calculated the following skill scores: $KSS = 0.500$, $POD = 0.500$, $F = 0.000$ and $PC = 0.778$. However, her independent test was based on only nine observed storms (four of which were super-intense and five intense).

These comparisons also indicate that our NN model has a forecasting ability comparable to the older published models, possibly even slightly better. However, we must not forget that our forecasts were restricted to the days on which the hourly values of the vertical IMF component B_z were negative at least 16 times. This represents a significant difference, which we shall take into account in interpreting the results in the following final section.

The condition of the long-lasting southern orientation of the north-south component B_z of the IMF is essential in our study. It enabled us to study the situation in which the Earth's magnetosphere is very responsive to the disturbances of the solar wind (so-called open magnetosphere). If the neural network had been trained using the same inputs and employing all days (not only the days with 16 or more negative values of B_z), the network would have been confused by ambiguous training patterns because similar or very same input values would have corresponded to different desired outputs: the like input values would have been requested to yield higher level of the geomagnetic activity for the open magnetosphere and lower activity for the "closed" magnetosphere. The resulting skill scores (KSS, POD, F and PC) would consequently have been worse than the scores that we obtained in our study.

The assessment of our NN model is to some extent restricted due to small number of the independent test patterns, especially for cases C9 ≥ 8 (Table 2). It is because we needed to employ most of the patterns for the training of the NNs and some patterns were used for the validation (Sub-section 3.3). In addition, some days of the studied period were excluded from the analysis due to incomplete records. Additional data will be required in future studies from subsequent solar activity cycles (at least one more complete one) to improve statistical significance of our results.

5. Discussion and conclusion

The purpose of this paper was to point out the possibilities of mid-term forecasts of the danger of high geomagnetic activity under the assumption that the orientation of the vertical IMF component is unpredictable (at least not with a lead time of the order of days). We solved the problem in two steps.

In the first step, we studied the hourly averages of the north-south component B_z of the IMF in connection with the daily level of GA expressed in terms of index C9. We found that very high GA (C9 > 7) usually develops if, on the day in question, the southern orientation of the IMF lasted for at least 16 hours, i.e. the average values of B_z were negative at least 16 times. On these days the C9 index was one level higher than on other days. In particular, on these days the median of C9 was equal to 3, whereas on the other days the median of C9 was equal to 2.

This means that, if we wish to forecast potentially dangerous high geomagnetic activity, we should concentrate on forecasts assuming that, at the time of arrival of the CME at the Earth, B_z is oriented southwards for at least 16 hours. We thus obtain a kind of upper estimate, which will tell us how high a GA is threatening the Earth should the ICME hit the Earth under the "most sensitive" conditions in the configuration of magnetic fields. This was the key idea in our paper.

In the second step, we suggested using artificial neural networks in forecasting the danger of high GA. This method is not new in forecasting GA. However, the approach is new in that we used the days, on which the configuration of the magnetic fields was favorable for developing severe geomagnetic storms, as patterns to train the networks: we forecast the GA for days on which at least 16 hourly averages of B_z were negative. In our approach we cannot give an assurance that a strong magnetic storm is going to happen, instead we can announce that there is the threat of coming the strong storm. At the same time we can tell that such a storm will strike with the 31% probability.

We tested the model and compared the results of the test with the results of authors of similar papers (see Section 4). Most indices indicate that our results are better than those published earlier. The compared models, however, did not deal with exactly the same problem. Hence, the comparison is only of informative value. We can thus consider the statistical assessment of our results a precedent with which future studies focused on forecasting the danger of high GA under dominant southern orientation of the IMF can be compared. Nevertheless, more robust statistics for supporting our conclusions would require more extensive series of test data, which would be available probably at the end of the new solar cycle.

Acknowledgements

This work was supported in part by VEGA grants 2/0022/11 and 2/0015/11 of the Scientific Grant Agency of the Ministry of Education of Slovak Republic and the Slovak Academy of Sciences, by the Slovak Research and Development Agency under the contract No. APVV-0662-12, by the grant of the ASCR under project IAA300120608 and by the Ministry of Education, Youth and Sports of the Czech Republic under project OC09070.

References

References

ACE Science Center, URL (cited on 23/01/2012): www.srl.caltech.edu/ACE /ASC/level2/new/ACEL2Server.cgi?datasetID=mag_level2_data_1hr, 2012.

Andrejkova, G., Toth, H., Kudela, K., Fuzzy neural network in the prediction of geomagnetic storm. AI Application in Solar-Terrestrial Physics, ESA WPP-148, pp. 173-179, 1998.

Boberg, F., Wintoft, P., Lundstedt, H., Real time Kp predictions from solar wind data using neural networks. Phys. Chem. Earth, 25, 275-280, 2000.

Bochníček, J., Hejda, P., Valach, F., Solar energetic events in the years 1996-2004. The analysis of their geoeffectiveness, Studia Geophysica et Geodaetica 51 (3) , 439-447, 2007.

Bothmer, V., Schwenn, R., The structure and origin of magnetic clouds in the solar wind, Annales Geophysicae 16 (1) , 1-24, 1998.

Chen, J., Cargill, P.J., Palmadesso, P.J., Real-time identification and prediction of geoeffective solar wind structures, Geophysical Research Letters, 23, 6, 625-628, 1996.

Chen, J., Slinker, S.P., Triandaf, I., Bayesian prediction of geomagnetic storms: Wind data, 1996-2010, Space Weather, 10, S04005, doi:10.1029/2011SW000740, 2012.

Cliver, E.W., Hudson, H.S., CMEs: How do the puzzle pieces together? J. Atmos. Terr. Phys., 64, 231-252, 2002.

Demuth, H., Beale, M., Hagan, M., Neural Network Toolbox 5, User's Guide, The MathWorks, Natick, 2005-2007.

Dryer, M., Comments on the origins of coronal mass ejections. Sol. Phys., 169, 421-429, 1996.

Gleisner, H., Watermann, J., Solar energetic particle flux enhancement as an indicator of halo coronal mass ejection geoeffectivness, Space Weather, 4, S06006, doi:10.1029/2006SW000220, 2006.

Gleisner, H., Watermann, J., Concepts of medium-range (1 – 3 days) geomagnetic forecasting, Adv. Space Res., 37, 1116– 1123, 2006.

Gopalswamy, N., Yashiro, S., URL (cited on 23/01/2012): http://cdaw.gsfc.nasa.gov/CME_list/, 2012.

Gopalswamy, N., Yashiro, S., Michalek, G., Stenborg, G., Vourlidas, A., Freeland, S., Howard, R., The SOHO/LASCO CME Catalog, Earth, Moon, and Planets 104 295-313, doi:10.1007/s11038-008-9282-7, 2009.

Gurney, K., An Introduction to Neural Networks. UCL Press, London, 1997.

Harrison, R.A., Coronal magnetic storms: A new perspective on flares and the "flare myth" flare myth debate. Sol. Phys., 166, 441-444, 1996.

Hertz, J., Krogh, A., Palmer R.G., Introduction to the Theory of Neural Computation. Addison-Wesley, Reading, MA, 1991.

Howard, T., Coronal Mass Ejections: An Introduction. Springer, New York, Dordrecht, Heidelberg, London, doi:10.1007/978-1-4419-8789-1, 2011.

Jankovičová, D., Dolinský, P., Valach, F., Vörös Z., Neural network-based nonlinear prediction of magnetic storms. J. Atmos. Sol.-Terr. Phys., 64, 651-656, 2002.

Kahler, S.W., Cliver, E.W., Ling, A.G., Validating the proton prediction system (PPS), Journal of Atmospheric and Solar-Terrestrial Physics 69, 43-49, 2007.

Kosugi, T., Shibata, K., Solar coronal dynamics and flares as a cause of interplanetary disturbances. In: B.T. Tsurutani, W.D. Gonzales, Y. Kamide and J.K. Arballo (Eds), Magnetic Storms. Geophysical Monograph, 98, AGU Press, Washington D.C., 21-34, 1997.

Kugblenu, S., Taguchi, S., Okuzawa, T., Prediction of the geomagnetic storm associated Dst index using an artificial neural network algorithm, Earth Planets Space, 51, 307-313, 1999.

Lundstedt, H., Wintoft, P., Prediction of Geomagnetic Storms from Solar Wind Data with Use of a Neural Network. Ann. Geophysicae 12, 19-24, EGS-Springer-Verlag, 1994.

Lundstedt, H., Gleisner, H., Wintoft, P., Operational forecasts of geomagnetic Dst index. Geophys. Res. Lett., 29, 2181, doi: 10.1029/2002GL016151, 2002.

McAllister, A.H., Martin, S.F., Crooker, N.U., Lepping, R.P., Fitzenreiter, R.J., A test of real-time prediction of magnetic cloud topology and geomagnetic storm occurrence from solar signatures, J. Geophys. Res., 106(A12), 29,185-29,194, doi:10.1029/2000JA000032, 2001.

National Geophysical Data Center, URL (cited on 23/01/2012): ftp://ftp.ngdc.noaa.gov/STP/GEOMAGNETIC_DATA/INDICES/KP_AP, 2012.

NOAA Space Environment Center, Boulder, URL (cited on 23/01/2012): http://www.swpc.noaa.gov/ftpmenu/indices/events.html, 2012.

Schmid, M.D., A Neural Network Package for Octave, User's Guide, Version: 0.1.9.1, URL (cited on 05/10/2010): http://plexso.com/61_octave/neuralNetworkPackageForOctaveUsersGu.pdf, 2009.

Schwenn, R., Space weather: The solar perspective, Living Rev. Solar Phys. 3, lrsp-2006-2, 2. URL (cited on 06/08/2012): http://www.livingreviews.org/lrsp-2006-2, 2006.

Srivastava, N., A logistic regression model for predicting the occurrence of intense geomagnetic storms, Ann. Geophys., 23, 2969– 2974, 2005.

Stepanova, M., Antonova, E., Muños-Uribe, F.A., Gomez-Gordo, S.L., Torres-Sanchez, M.V., Prediction of geomagnetic storm using neural networks: Comparison of the efficiency of the satellite and ground-based input parameters, Journal of Physics: Conference Series, 134, 012041, doi:10.1088/1742-6596/134/1/012041, 2008.

Tian, J.H., Zhang, J.C., Pu, Z.Y., Classification of solar wind structures and intense geomagnetic storm alarms with self-organizing maps, Advances in Space Research, 36, 2372-2377, 2005.

Tsurutani, B.T., The interplanetary causes of magnetic storms, substorms and geomagnetic quiet. In Space Storms and Space Weather Hazards, ed. by I.A. Daglis, Kluwer Academic Publisher, Dordrecht, Boston, London, 103-130, 2001.

Tsurutani, B.T., Gonzalez, W.D., Zhou, X.-Y., Lepping, R.P., Bothmer, V., Properties of slow magnetic clouds, J. Atmos. Sol.-Terr. Phys., 66, 147-151, 2004.

Valach, F., Hejda, P., Bochníček, J., Geoeffectiveness of XRA events associated with RSP II and/or RSP IV estimated using the artificial neural network, Stud. Geophys. Geod., 51, 551-562, 2007.

Valach, F., Revallo, M., Bochníček, J., Hejda, P., Solar energetic particle flux enhancement as a predictor of geomagnetic activity in a neural network-based model, Space Weather, 7 (4), art. no. S04004, doi: 10.1029/2008SW000421, 2009.

Valach, F., Revallo, M., Hejda, P., Bochníček, J., Predictions of SEP events by means of a linear filter and layer-recurrent neural network, Acta Astronautica 69, 758-766, 2011.

Wu, J.-G., Lundstedt, H., Geomagnetic storm predictions from solar wind data with the use of dynamic neural networks, Journal of Geophysical Research, 102, A7, 14457-14466, 1997.

Yurchyshyn, V.B., Wang, H., Goode, P.R., Deng, Y., Orientation of the Magnetic Fields in Interplanetary Flux Ropes and Solar Filaments, The Astrophysical Journal, 563, 381-388, 2001.

Zhao, X.P., Hoeksema, J.T., Marubashi, K., Magnetic cloud B_s events and their dependence on cloud parameters, J. Geophys. Res., 106(A8), 15, 643-15, 656, doi:10.1029/2000JA000421, 2001.

Table 1: Contingency table and assessment of the successfulness of forecasting high geomagnetic activity (C9 = 7, 8 or 9) in terms of skill scores KSS, POD, F and PC.

Forecast high GA	Occurence of high GA: yes	Occurence of high GA: no	
yes	11	5	$KSS = 0.463$
no	11	129	$POD = 0.500$
			$F = 0.037$
			$PC = 0.897$

Table 2: Contingency table and assessment of the successfulness of forecasting high geomagnetic activity (C9 = 8 or 9) in terms of skill scores KSS, POD, F and PC.

Forecast high GA	Occurence of high GA: yes	Occurence of high GA: no	
yes	4	11	$KSS = 0.727$
no	1	140	$POD = 0.800$
			$F = 0.073$
			$PC = 0.917$

Table 3: The contingency table describing the successfulness of forecasting the daily level of GA, expressed in terms of index C9 in the independent final test. Our model is unable to distinguish the degrees of GA for medium and weak GA. However, the classification into two categories can be seen, i.e. “yes/no” for the occurrence of high GA with the limiting value C9 = 7. (Due to lucidity, we used a bold font for the quantities greater than or equal to two.)

Forecast value of C9	Observed value of C9: 0	1	2	3	4	5	6	7	8	9
0	**11**	**20**	**20**	**19**	**14**	**11**	**14**	**9**	0	0
1	0	1	0	1	0	**2**	0	0	0	0
2	0	**2**	**3**	1	0	0	0	1	0	0
3	0	0	**3**	0	0	0	0	0	0	0
4	1	1	1	0	1	1	0	0	0	0
5	0	0	0	0	1	0	1	1	0	0
6	0	0	0	0	0	0	0	0	0	0
7	0	0	0	0	0	0	0	0	0	1
8	0	0	0	0	1	1	0	0	0	0
9	0	1	0	0	0	0	**2**	**6**	**2**	**2**

Figure 1: Result of data survey analysis. This expresses the number of times the hourly average of B_z was negative on the given day for the separate daily averages of GA C9 = 0, 1, 2, ... , 9. The box-and-whisker diagrams provide information on the smallest and largest values in the statistical sub-set, on the bottom and top quartile and on the median. The number of cases in the sub-set is given at each box. The dashed line marks the threshold value separating the days with very high GA.

Figure 2: Quartile statistics for GA (index C9) if the hourly average of B_z on the given day is negative less than 16 times (l.h. box-and-whisker diagram) and if B_z is negative at least 16 times (r.h. diagram). The number of items in the individual sub-sets is shown above each box.

Figure 3: Input quantities of the neural network, consisting of both CME and X-ray flare data described in Sub-section 3.1, (l.h.s. of figure), architecture of the neural network, and the output quantity, the forecast C9 index, (r.h.s. of figure).

Figure 4: The number of hidden neurons contained in the best neural networks for forecasting high GA with index C9 = 9 (l.h. diagram), C9 = 8 to 9 (middle diagram) and C9 = 7 to 9 (r.h. diagram) expressed with the aid of "whiskered boxes". At each box the number of NNs used to construct the diagram is shown: Based on the results of the validation test, we chose 17, 13 and 12 networks, respectively; yet 6 of the networks simultaneously occur in the first and second boxes. (We selected 36 various neural networks, all told.)

This is the author's version of a manuscript that was accepted for publication in Advances in Space Research. The definitive version was subsequently published in:
Fridrich Valach, Josef Bochníček, Pavel Hejda and Miloš Revallo: Strong geomagnetic activity forecast by neural networks under dominant southern orientation of the interplanetary magnetic field.
Advances in Space Research, VOL 53, ISSUE 4, PAGES 589-598, 2014. DOI: 10.1016/j.asr.2013.12.005

Figure 1

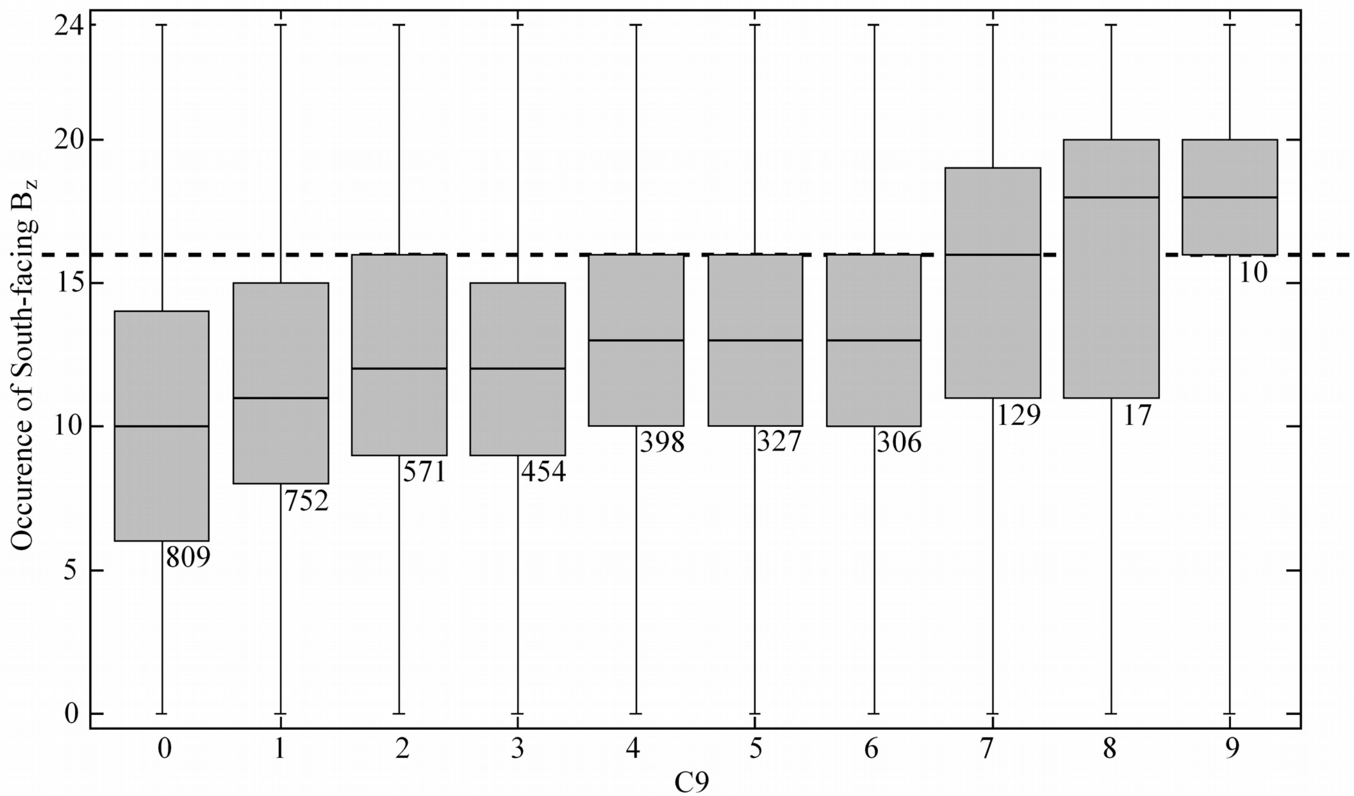

Fridrich Valach, Josef Bochníček, Pavel Hejda and Miloš Revallo: Strong geomagnetic activity forecast by neural networks under dominant southern orientation of the interplanetary magnetic field.
Advances in Space Research, VOL 53, ISSUE 4, PAGES 589-598, 2014. DOI: 10.1016/j.asr.2013.12.005

Figure 2

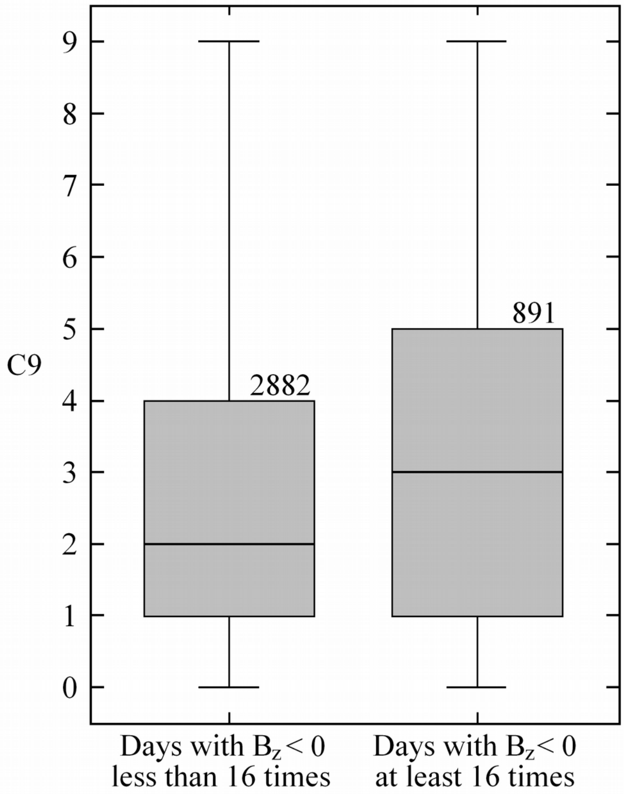
C9
0
1
2
3
4
5
6
7
8
9
2882
891
Days with $B_z < 0$
less than 16 times
Days with $B_z < 0$
at least 16 times

Figure 3

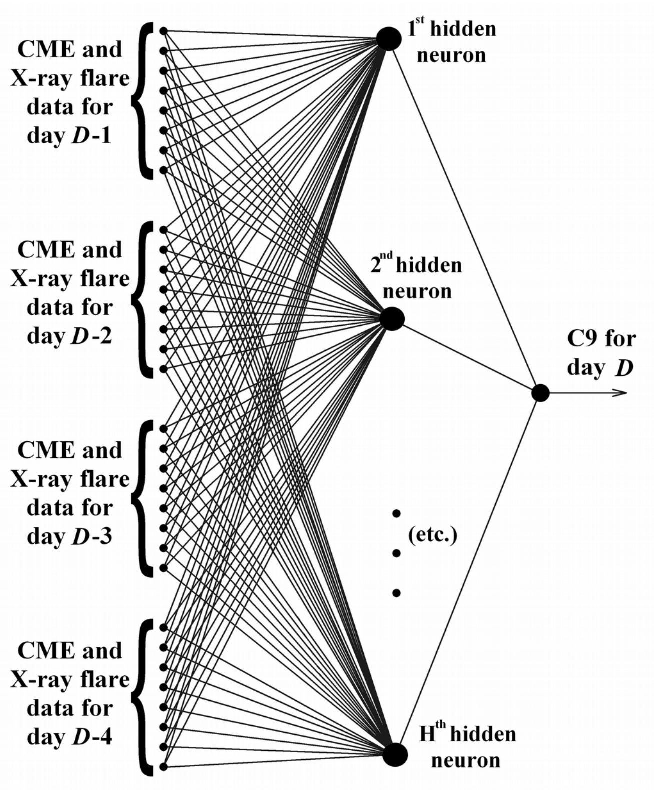

This is the author's version of a manuscript that was accepted for publication in Advances in Space Research. The definitive version was subsequently published in:
Fridrich Valach, Josef Bochníček, Pavel Hejda and Miloš Revallo: Strong geomagnetic activity forecast by neural networks under dominant southern orientation of the interplanetary magnetic field.
Advances in Space Research, VOL 53, ISSUE 4, PAGES 589-598, 2014. DOI: 10.1016/j.asr.2013.12.005

Figure 4

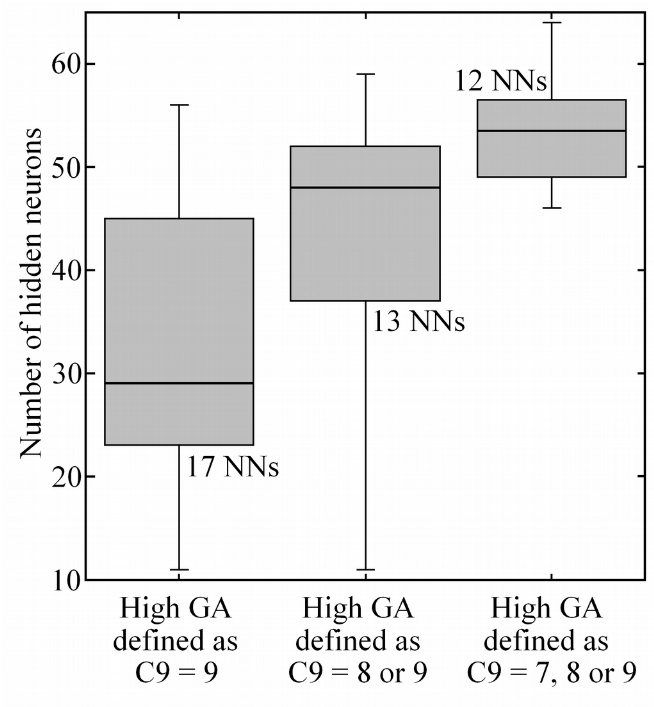

Fridrich Valach, Josef Bochníček, Pavel Hejda and Miloš Revallo: Strong geomagnetic activity forecast by neural networks under dominant southern orientation of the interplanetary magnetic field.
Advances in Space Research, VOL 53, ISSUE 4, PAGES 589-598, 2014. DOI: 10.1016/j.asr.2013.12.005